March 23, 2011

Effect of Stress State on Wrinkle Morphology

Derek Breid
Alfred Crosby, *University of Massachusetts - Amherst*

Soft Matter

Cite this: *Soft Matter*, 2011, **7**, 4490

www.rsc.org/softmatter

PAPER

Effect of stress state on wrinkle morphology†

Derek Breid and Alfred J. Crosby*

Received 28th January 2011, Accepted 4th March 2011
DOI: 10.1039/c1sm05152k

Wrinkles in thin films on soft substrates have been shown to self-organize into topological patterns, providing a possible route towards inexpensive generation of surface microstructure. However, the effect of the magnitude of applied stress in relation to the critical buckling stress, or overstress, on the observed patterns has until this point been neglected experimentally. In this paper, we investigate the effect of overstress using poly(dimethylsiloxane) which has been surface-oxidized with a UV-ozone oxidation technique. Using a swelling-based stress application technique, where the applied swelling stress in the thin film is controlled by changing the concentration of vapor-phase swelling agent (ethanol) in a sealed swelling chamber, we are able to impart swelling stresses below, at, and well above the critical stress. We observe a transition from hexagonally packed dimples at low overstress to ridge-based morphologies (herringbone and labyrinth) at high overstress. The observed dimple structures are remarkably widespread, and the hexagonal arrangement of these dimples is confirmed using Fourier analysis. Although analytical results predict that a square arrangement of dimples is preferred to hexagonal for flat wrinkling surfaces, hexagonal arrays are nonetheless unilaterally observed at low overstress. We attribute this observation to an inherent curvature that develops in the swelling film. The overstress is quantified by measuring the radius of curvature of swelling bilayer beams, both confirming the preferential swelling of the surface oxide layer by ethanol and quantifying the swelling extent. Effects of non-equibiaxial stress are investigated by inducing a compressive prestress prior to swelling, and "trapped" non-equilibrium morphologies are discussed briefly.

Introduction and background

A surface consisting of a thin, stiff film on a soft substrate undergoes a periodic out-of-plane buckling deformation when a compressive stress is applied at the interface of the two materials. This results in patterns of corrugated peaks and valleys on the surface, which, depending on the exact nature of the buckling process, can result in wrinkles,[1] folds,[2] creases,[3] or delaminations.[4,5] Wrinkles—characterized by their smooth sinusoidal surface contour—have shown particular ability to form well-ordered patterns with regular peak-to-peak spacing, consistent amplitude of deformation, and long-range pattern order.

Since the first experimental use of wrinkling as a patterning technique over a decade ago,[6] the concept has been applied towards the development of a diverse array of material applications, such as templating,[7–9] cell growth,[10] adhesion,[11,12] and optically active surfaces.[13,14] Additionally, wrinkling and buckling mechanisms are increasingly being suggested as routes for the formation of synthetic analogs that mimic complex topologies observed in many natural tissues: fingerprints,[15] arterial lining,[16] flowers,[17] leaves,[18] and fruits.[19] Yet, despite the wide variety of material systems and techniques thus far reported, understanding of the processes by which surfaces wrinkle is incomplete, particularly in regards to the observed morphological patterns of wrinkled surfaces at low stresses.

Neglecting kinetic factors, wrinkle morphologies are dictated by two primary factors: (1) the ratio of the magnitudes of the lateral principal stresses—specifically, whether or not the stress can be considered equibiaxial; and (2) the magnitude of the applied overstress relative to the critical threshold stress required for buckling. For elastic systems where the film thickness is small, the critical buckling stress is:[20]

$$\sigma_c = \frac{\bar{E}_f}{4}\left(\frac{3\bar{E}_s}{\bar{E}_f}\right)^{2/3} \quad (1)$$

At high overstress ($\sigma/\sigma_c \gg 1$), wrinkling systems tend to form ridges, where the local maxima and minima form continuous lines. The pattern that forms for a uniaxial stress is simply straight lines orthogonal to the axis of applied stress.[20] For equibiaxial stress conditions, experiments,[6,21] theory,[22–26] and simulation[26] unilaterally report the zigzag herringbone pattern

Polymer Science and Engineering, University of Massachusetts, Amherst, MA, USA. E-mail: crosby@mail.pse.umass.edu; Fax: +1 (413) 545-0082; Tel: +1 (413) 577-1313

† Electronic supplementary information (ESI) available: Additional images depicting prebuckling behavior, non-uniform wrinkling, buckling mode transitions, additional dimple structures and plot of dimple morphology as a function of ethanol fraction and overstress. See DOI: 10.1039/c1sm05152k

(or the labyrinth pattern, which is essentially a disordered herringbone[21,27]). At low overstress ($\sigma/\sigma_c \gtrsim 1$), patterns where the local maxima and minima are single points (*i.e.*, bumps and dimples) are both predicted and observed, but the geometric arrangement of these extrema are not consistent between theory and experiment. Theoretical calculations of the energy of deformation under equibiaxial stress suggest the formation of square 'checkerboard' arrays,[24,28] while experiments favor a hexagonal packing of dimples.[29–31] However, it is important to note that the applied stress in swelling-driven wrinkle experiments has not yet been quantified; therefore, quantitative comparison between experiments and theory has been not possible.

In this paper, we present experimental observations of wrinkle morphologies resulting across a wide range of applied stress magnitudes—from levels just above the critical buckling stress to levels of high overstress—for equibiaxial and non-equibiaxial stress states. These stresses are produced by the swelling of a thin capping layer generated by UV–ozone (UVO) oxidation of a poly(dimethylsiloxane) (PDMS) elastomeric substrate *via* absorption of solvent vapor. Control over the magnitude of these stresses is enforced by changing the vapor pressure of the solvent in the atmosphere, as well as the extent of oxidation. We quantify the applied swelling stress by fabricating beams of UVO-treated PDMS and measuring the curvature at equilibrium in a vapor atmosphere. With this methodology, we demonstrate the application of stresses that are simultaneously low-magnitude and equibiaxial, a condition which has otherwise been difficult to realize; thus permitting the identification of the conditions for hexagonal wrinkling morphologies.

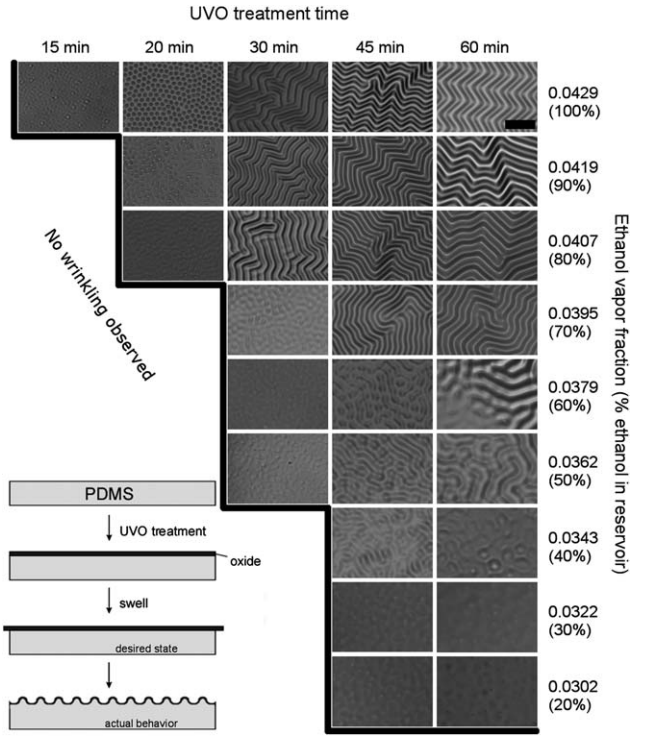

Fig. 1 (a) Observed wrinkle morphologies of swollen oxide films on PDMS substrates for various UVO treatment times and solvent vapor concentrations. No wrinkling was observed for vapor concentrations below the pictured images, or for UVO treatments shorter than 15 minutes. (b) Schematic of sample preparation and swelling mechanism. Scale bar represents 250 μm.

Results

Fig. 1 shows typical morphological features of the resulting wrinkled surfaces across the ranges of UVO time and ethanol percent after 24 hours absorption time. In these experiments, square slabs of PDMS (10 mm × 10 mm × 3 mm) were UVO-treated for 10–60 minutes and placed in solvent atmospheres above ethanol–glycerol reservoirs containing 10–100% ethanol by volume. A clear transition from ridges to dimples and then to no wrinkles is observed across the range of UVO times, particularly at 100% ethanol, with the dimple morphology emerging strongly at 20 minutes UVO. At 15 minutes differential interference contrast (DIC) microscopy reveals small amplitude undulations, which we will call "prebuckling", as the phenomenon is also seen to precede wrinkling in more highly swollen samples. This prebuckling is not observed prior to swelling. Although Fourier analysis of prebuckled surfaces indicates that the lateral length scale of these undulations is similar to the wrinkle wavelength (see the ESI†), they exhibit no regular ordering. We have used the emergence of a Fourier peak to indicate the presence of prebuckling in order to identify the critical buckling point, which we define as the lowest swelling for which prebuckling or wrinkling is observed. Similar prebuckling has been observed in simulations[27,33] and for wrinkling caused by thermal shrinkage.[34]

A similar—though less defined—transition occurs with decreasing ethanol vapor pressure. Although the ethanol vapor percent only changes from 4.2% to 2.8%, this is sufficient to observe the entire ridge-to-no wrinkling transition for 60, 45, and 30-minute UVO treatments. In contrast to the UVO-time transition, there is no single distinct dimple pattern. Rather, we observe a series of transitional phases containing characteristics of both ridges and dimples, or characteristics of both dimples and prebuckling. Unlike wrinkling at higher ethanol concentrations, which is quite consistent across the entire surface, the wrinkling observed in this regime (45–60 min UVO time, 40–60% ethanol) tends to vary across the surface, with some regions buckling into ridges and some regions remaining flat (see the ESI†). In between are transitional regions of varying width—in some cases the ridges abut the flat regions, while other transitional regions were on the same lateral size-scale of the ridged and flat regions. Overall, the extent of wrinkling decreased visibly with decreasing vapor pressure—areal coverage of ridged regions decreased, and apparent amplitudes of all observed morphologies diminished.

The observed inhomogeneity of the wrinkling process under conditions of reduced swelling indicates that local stresses may vary in magnitude across the surface of the sample. Furthermore, it suggests these swelling stresses may not necessarily remain equibiaxial during the entire formation history, particularly at the critical point where buckling initiates. Typically, this stress inequality is directly associated with sample edges or visible surface defects in the film (Fig. 2a). To observe the direct influence of a range of non-equibiaxial stress distributions under similar wrinkling conditions, simple experiments were conducted in which the compressive stress in the film was directionally biased. The effect of deviance from perfectly equibiaxial stress on

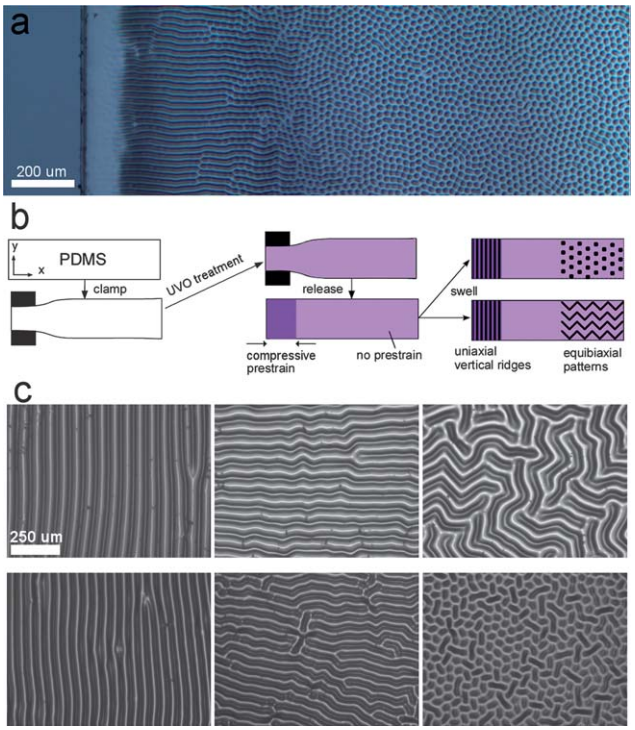

Fig. 2 (a) Image of wrinkling at the edge of a sample for UVO treatment of 20 minutes at 100% ethanol. Near the edge, the swelling stress becomes non-equibiaxial, resulting in the formation of uniaxial ridges. (b) Schematic of the clamping process used to induce a uniaxial prestress in one end of a beam prior to wrinkling. (c) Optical micrographs of the center of the prestressed samples (sample width = 5 mm) at swelling equilibrium for UVO treatment times of 20 and 30 minutes, with details of the wrinkle morphology at selected points.

the wrinkle morphology for two different UVO treatment times is shown in Fig. 2c. In these experiments, one end of a long PDMS beam was clamped during UVO exposure (Fig. 2b). The clamping was applied horizontally, such that the face receiving oxidation was not masked by the clamp and still received the full dose of oxidation. Upon release from the clamp, a compressive stress developed in the oxide layer along the long axis of the beam.

However, the magnitude of this stress remained below the critical buckling stress, and no wrinkling was observed at this point. The samples were then placed into a sealed vapor chamber. After the samples had equilibrated in the vapor atmosphere, the wrinkles which developed in the prestressed regions were aligned orthogonally to the long (x) axis of the beam, consistent with the direction of the compressive prestress. Far away from the clamped end, the expected equibiaxial patterns were recovered: labyrinth for high overstress and dimples for low overstress. Between the two ends is a third region where the wrinkles formed into long ridges aligned *parallel* to the long axis, indicating a compressive prestress in the y direction. Thus, traveling along the long axis of the beam shows a gradual transition from ridges aligned perpendicular to the axis to ridges aligned parallel, which then transit into either a dimple or labyrinth pattern (see the ESI† for stitched images depicting the entire beam surface). For the sample with higher overstress (30 minutes UVO), the transition from ridges to labyrinth actually proceeds through the herringbone pattern—as the stress becomes more equibiaxial, periodic jogs in the ridges are observed, which grow in sharpness as the distance from the clamped end continues to increase. Conversely, for the sample with lower overstress (20 minutes UVO), the transition from ridges to dimples happens more abruptly: there is a short region where ridges and dimples mix, then dimples completely dominate the surface, though there does seem to be some further distance over which the ridges influence the exact locations of the dimples. Also, the dimples were observed to coalesce, indicating that swelling stress continued to increase beyond that which led to dimple formation.

Simple finite element simulations of an elastic beam compressed at one end illustrate the stress profile along the long axis of the beam. Fig. 3a depicts σ_{xx} and σ_{yy} at the center of the top surface of the beam, as a function of lateral position along

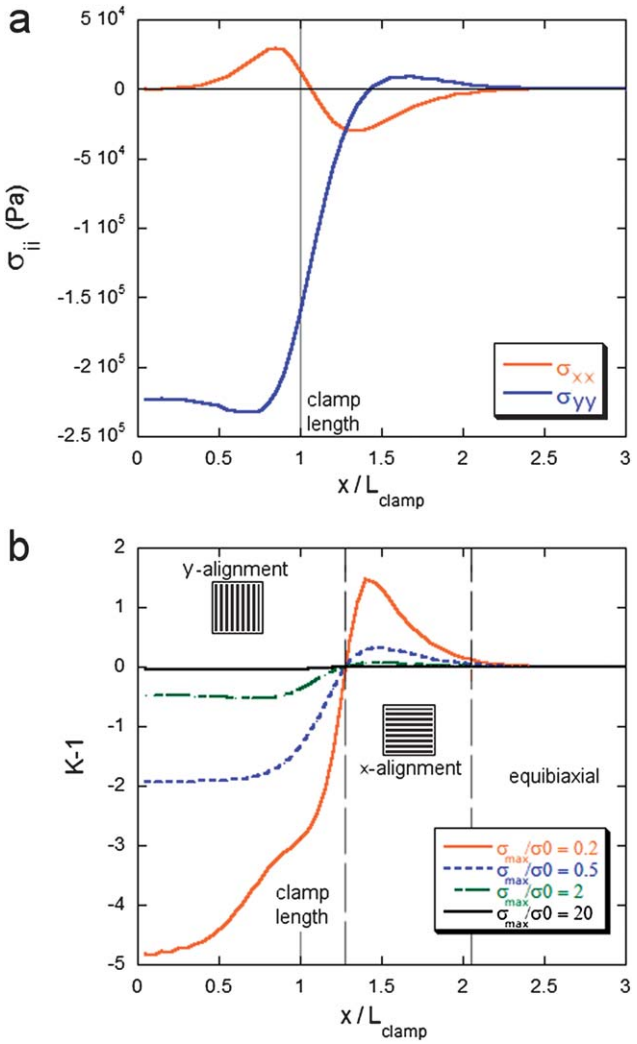

Fig. 3 (a) Finite element stress profiles at the center of the top surface of a modeled clamped elastic beam as a function of length along the long (x) axis, using the directional naming convention depicted in Fig. 2b. Here, tensile stresses in one direction result in the formation of orthogonally aligned wrinkles. (b) Plot of $K - 1$ as a function of x for selected values of σ_{max}/σ_0.

the x axis. Since the simulation represents the compression of the beam before oxidation, tensile stresses correspond to compressive stresses in the released beam, which direct orthogonal wrinkle alignment. Therefore, the positive stresses in the clamped region confirm the experimentally observed wrinkle alignment. In addition, the observed transition from y-aligned wrinkles within the clamped region to x-aligned wrinkles around the beam's midpoint is seen, as the beam is put into tension in the y-direction in this region.

To illustrate the effect of an additional swelling stress on top of the applied prestress in determining wrinkle directional bias, an equibiaxial tensile stress σ_0 is added to both σ_{xx} and σ_{yy}. The ratio of these two sums:

$$K = \frac{\sigma_{yy} + \sigma_0}{\sigma_{xx} + \sigma_0} \tag{2}$$

is plotted in Fig. 3b as a function of axial position for different values of σ_0 normalized by the overall maximum stress magnitude from Fig. 3a. It is immediately apparent that the observed wrinkle orientation is verified over all values of σ_0, as $(K-1) < 1$ favors y-oriented wrinkles while $(K-1) > 1$ favors x-orientation. When $(K-1) = 0$, the stress state is, of course, equibiaxial and no preferred orientation occurs. As expected, the magnitude of $(K-1)$ is greatest when σ_0 is small relative to the modeled stress values, allowing the clamping prestresses to dominate. As σ_0 becomes large compared to the clamping stress, it becomes the dominant term, driving K towards unity and minimizing the effect of prestress.

To quantify the effect of overstress on the wrinkling patterns, we measured the applied swelling stress *via* beam bending experiments. Beams of PDMS measuring 15 mm × 3 mm and ranging from 165–535 μm in thickness were fabricated. These films were UVO-treated for between 10 and 60 minutes, and subsequently hung vertically in the vapor atmosphere. Upon swelling, the beams curled due to the differential strain induced by differences in the swelling extent of the oxidized film and the non-modified PDMS. Fig. 4 shows an example of an oxidized beam curling when exposed to ethanol vapor. The direction of the curl confirms that the ethanol swells the oxide film to a greater extent as compared to the unmodified PDMS, a somewhat surprising result, for the oxide material is considered to be nearly glass-like.[35] However, it is a hydrophilic material, so an affinity for polar solvents is not unexpected. To further confirm the specificity of this swelling difference, swelling in hexane vapor was also conducted. Hexane induces a sign reversal of the curvature compared to ethanol, for it is a well-known solvent and swelling agent for PDMS.

The radius of curvature of these beams can be related to the differential strain, $\varepsilon_{\text{diff}}$ at the interface of the bilayer through the classic bending bilayer problem:[36,37]

$$\frac{h_1}{R} = \frac{2\frac{E_2}{E_1}\times\frac{h_2}{h_1}\left(1+\frac{h_2}{h_1}\right)\varepsilon_{diff}}{1+\left(\frac{E_2}{E_1}\times\frac{h_2^2}{h_1^2}\right)^2+2\frac{h_2}{h_1}\times\frac{E_2}{E_1}\left(2+3\frac{h_2}{h_1}+2\frac{h_2^2}{h_1^2}\right)} \tag{3}$$

here, h is the layer thickness and E is the Young's modulus. We define PDMS as material 1, and the oxide film as material 2. According to previous measurements of UVO-treated PDMS,[35] we expect (h_2/h_1) to be relatively small (<0.01). Therefore higher order terms are neglected, and eqn (3) simplifies to:

$$\varepsilon_{\text{diff}} \approx \left(\frac{h_1}{R}\right)\left(2+\frac{E_1 h_1}{E_2 h_2}\right) \tag{4}$$

A more useful representation of this curvature is to reframe it in terms of the extent of applied overstress (σ/σ_c) relative to the critical buckling stress. We define the critical buckling point for a given UVO time as the lowest ethanol concentration for which any buckling, including prebuckling, is observed. The critical buckling concentration was determined from the wrinkling experiments depicted in Fig. 1. Consequently, $(h_1/R)_c$ is defined as the measured beam strain at that critical point. Since the maximum strain scales as (h_1/R), and the materials are assumed to behave in a linear elastic manner at low strains, we can write

$$\frac{\sigma}{\sigma_c} = \frac{\varepsilon}{\varepsilon_c} = \frac{(h_1/R)}{(h_1/R)_c} \tag{5}$$

Using the definition in eqn (5), we quantify the applied overstress for UVO time/ethanol concentration combinations by measuring the curvatures of the bilayer beam at both the specified and critical conditions. This overstress ratio is plotted in Fig. 5. There is a narrow range of prebuckling from $1 < \sigma/\sigma_c < 1.3$, above which there is another narrow range $(1.3 < \sigma/\sigma_c < 1.5)$ where a mixture of prebuckling and dimples are observed.

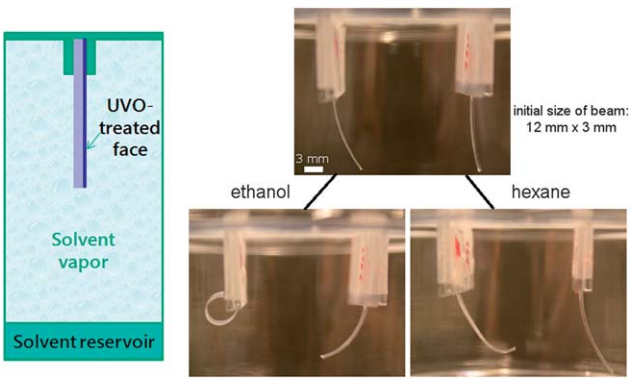

Fig. 4 Schematic of UVO-treated PDMS beam curling experiments, and example photographs of initial beam curvature and final curvature after exposure to ethanol and hexane for two different PDMS thicknesses, 165 μm and 330 μm.

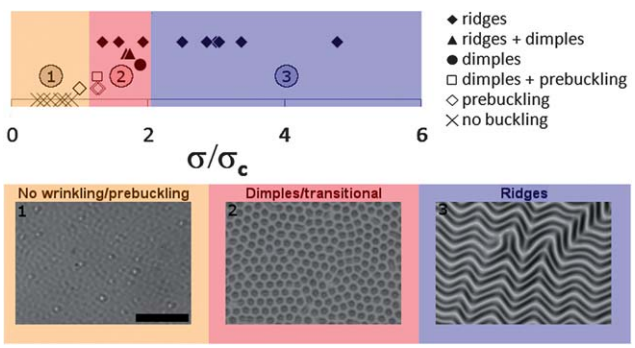

Fig. 5 Plot of wrinkle morphology as a function of overstress. Data points have been vertically offset for clarity.

Dimples alone occur at only one point (UVO time 20 min, 100% ethanol), at $\sigma/\sigma_c = 1.9$. Otherwise, for $\sigma/\sigma_c > 1.5$ either ridges or a mixture of ridges and dimples are observed. It should be noted that the single data point indicating dimples does not imply a single condition for which dimples may be observed. Fig. S3 in the ESI† shows other observations within the small range of conditions which lead to dimple formation.

Discussion

The morphology of wrinkled deformations associated with biaxial stress states is primarily dictated by two factors: (1) the ratio of the two in-plane principal stresses (σ_I and σ_{II}) and (2) the applied overstress, or magnitude of the applied stress as compared to the critical buckling stress. The dimple morphology is sensitive to both of these factors, emerging only when both the ratio of principal stresses is no greater than 1.1 and the overstress is less than 2, with ridges or a mix of ridges and dimples forming in the absence of either these conditions.

In a recent paper, Cai *et al.*[24] considered the energy of equilibrium wrinkle morphologies as a function of overstress under equibiaxial stress conditions ($\sigma_I = \sigma_{II}$). At high overstresses, they concluded that the herringbone pattern resulted in the lowest energy of any of the morphologies considered, in agreement with previous work.[23,25] Our observations at high overstress reflect this prediction to an extent: herringbone order is certainly present, but the wrinkled surfaces also exhibit considerable defects in this order. When the defects dominate (Fig. 1, 45 min UVO and 70% ethanol), the resulting pattern is known as the labyrinth morphology, and exhibits a system energy approaching that of the herringbone.[27] The labyrinth pattern typically emerges when the wrinkle initiation occurs homogeneously across the entire surface[21,27] under conditions where the herringbone pattern would otherwise be predicted. In fact, when the same stresses are applied in a heterogeneous manner, such as subsequent mechanical compression[21] or by a lateral swelling diffusion front,[38] a very well-ordered herringbone pattern results. In our experiments, the most highly ordered herringbone patterns occur near the edges of samples treated at high UVO times, suggesting wrinkle formation *via* an advancing front, a mechanism supported by previous observations of solvent-induced wrinkling.[29]

At low overstresses, the ranking of the buckling modes considered by Cai *et al.* is markedly different than at high overstress. In particular, the herringbone pattern is not among the critical buckling modes of an equibiaxially stressed system (*i.e.* modes that satisfy $\sqrt{k_1^2 + k_2^2} = k_c$, where k_c is the critical wavenumber); therefore, its energy must increase above these critical modes at some overstress $\sigma/\sigma_c > 1$. Although they show that the energetically minimal pattern in the low overstress regime should result in a square or "checkerboard" dimple array, our surfaces exhibit hexagonal ordering. Remarkably, these hexagonal dimples cover the entire wrinkling surface with no prepatterning, where prior reports[29] using this method required patterning of finite wrinkling plates to achieve dimples. Fig. 6 shows an example of the persistence of this pattern across a wide area. The hexagonal ordering emerges strongly over local areas covering several to tens of wavelengths, as seen by the fast Fourier transform over selected areas of the image. As the area of interest grows, perfection of a hexagonal lattice diminishes, and grains of local hexagonal order are defined, similar to those observed in hexagonally packed cylindrical block copolymers. Improvements in the hexagonal ordering may be possible by imposing macropatterning onto the surface prior to wrinkling, as has been shown for block copolymers.[39]

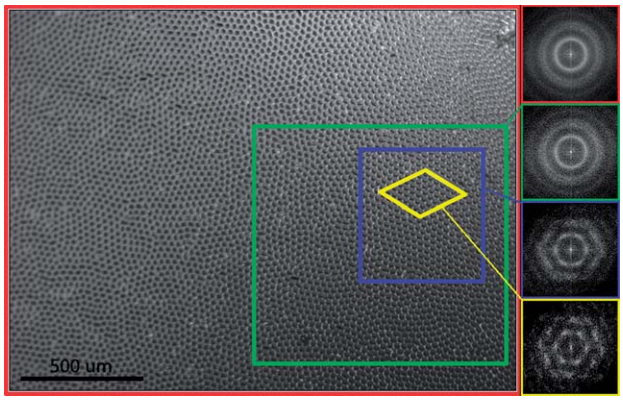

Fig. 6 Optical micrograph of laterally extensive dimple patterns. On the right are fast Fourier transforms of the indicated regions. The image as a whole exhibits a characteristic wavelength, but no long-range order. As the region of interest becomes smaller, the hexagonal ordering becomes stronger.

The hexagonal dimple arrays observed in our experiments differ from the predictions for low overstress in flat wrinkling systems of Cai *et al.*[24] and Audoly and Boudaoud[25] in two ways: (1) we observe hexagonal packing, instead of the predicted square packing and (2) we observe that the hexagonal structures always buckle into the substrate as dimples, rather than buckling out as convex bumps. Energetically, hexagonal arrays of dimples and bumps are equivalent for flat substrates.[24] However, if the wrinkling film is not flat, and instead begins with some finite inherent curvature, the energy of the hexagonal buckling mode bifurcates into two distinct cases depending whether the central hexagons are buckled into the surface or out of it. For a surface with convex curvature, dimples are energetically preferable to bumps. The magnitude of the bifurcation of the energies between the two cases depends on both the material properties and geometric parameters of the buckling film, and can be determined by a dimensionless curvature parameter:[24]

$$\Omega = 2\sqrt{\left(1 - \nu_f^2\right)}\frac{t}{R}\left(\frac{\bar{E}_f}{3\bar{E}_s}\right)^{2/3} \quad (6)$$

For sufficiently large Ω, the hexagonal dimple mode becomes the lowest-energy of any of the critical modes. Furthermore, the value of Ω at which the energies for the hexagonal and checkerboard modes are equal (Ω_{trans}) shows a strong dependence on the overstress, becoming quite small as σ/σ_c approaches unity. Thus, we must consider the possibility that a small initial substrate curvature may be causing the film to buckle into a hexagonal dimple pattern. For samples with a UVO treatment of 60 minutes, we observe the presence of hexagonal dimples at $\sigma/\sigma_c = 1.3$. However, it is reasonable to assume that the selection of buckling mode occurred at a lower overstress of $\sigma/\sigma_c \approx 1.1$.

According to Cai, the value of Ω_{trans} at this overstress is ~0.025. Eqn (6) can be re-expressed in terms of the wavelength of the hexagonal mode, $\lambda = \left(\frac{4}{\sqrt{3}}\right)\pi k$:

$$\Omega = \frac{3\sqrt{\left(1-\nu_f^2\right)}}{8\pi^2}\frac{\lambda^2}{t} \quad (7)$$

Using $\Omega = 0.025$, $\lambda = 40$ μm (Fig. 1), and = 100 nm,[35] we calculate $R \approx 26$ mm. A sample width of 10 mm would yield a rise of 0.5 mm at the center relative to the edge if this curvature was imposed upon the entire sample. If instead the curvature was caused by localized undulations in the swelling film, an even smaller rise would occur. Although we have not attempted to measure an induced curvature of the sample at the point of buckling, it is not unreasonable to suggest that curvatures of this magnitude do occur during our swelling experiments.

Though this report highlights the formation of laterally extensive hexagonal dimple arrays *via* wrinkling as a novel mechanism for lithography-free generation of surface topography, many patterns in nature are thought to form *via* a similar pathway. Li *et al.*,[40] have shown the patterned growth of spherules onto hexagonal lattices on the surface of a stressed core–shell microstructured hemisphere, noting similarities to seed-packing structures in nature, such as dandelions. The same material system was also used to generate hexagonally packed dimples on the surface of buckling core–shell spherical microparticles with high curvature.[41] An analytical model of fingerprint formation concludes that even surfaces with moderate curvature (~1 mm) prefer to organize into dimple structures instead of ridges,[15] suggesting such dimple formation as the mechanism driving formation of the palm-prints of koalas.

Finally, we wish to emphasize that the patterns presented in this paper represent the observed *equilibrium* morphologies of our wrinkling system. Beyond these patterns exists a wide array of "trapped" morphologies—patterns for which the system energy is not minimized, but may nonetheless be stable over long times due to kinetic considerations. One example already mentioned is the labyrinth pattern (Fig. 7a), which essentially represents a disordered version of the herringbone. A related pattern is the "segmented labyrinth" (Fig. 7b), which begins as an array of hexagonal dimples that coalesce as the overstress increases above the point where the herringbone pattern is most energetically stable. The dimples rarely coalesce beyond groups of two or three, and coalescence occurs randomly across the surface, resulting in no long-range organization, similar to the labyrinth pattern. However, occasionally dimple coalescence results in patterns with some persisting local order, resembling "cages" or "segmented herringbones" (Fig. 7b, inset). Using solvents which swell the oxide layer quickly often results in kinetically trapped structures with a large degree of order that appear to be related to the herringbone pattern, as they contain wrinkle features which are arranged orthogonally into periodic shapes. For example, oxide surfaces swollen with tetrahydrofuran (THF) vapor first form large areas of uniaxially aligned wrinkles which quickly transform into "zipper" patterns (Fig. 7c). Similar patterns were reported by Chan and Crosby for films swollen with liquid-phase acrylate monomers,[42] and the formation of perpendicular features in the midst of parallel wrinkles has been reported for mechanical compression.[43]

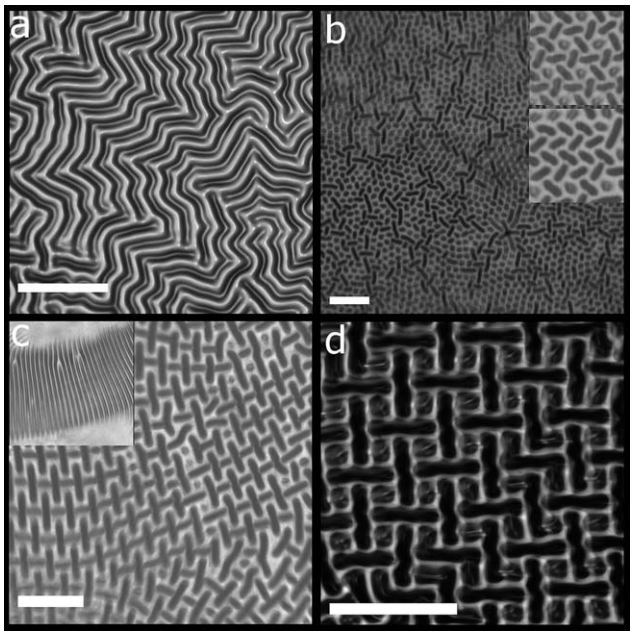

Fig. 7 Optical micrographs of various non-equilibrium morphologies as described in the text. (a) Labyrinth pattern. (b) Segmented labyrinth pattern; (inset, top): cage pattern; (inset, bottom): segmented herringbone pattern. Inset widths are 300 μm. (c) Zipper pattern; (inset): the same location at early stages of buckling, showing uniaxial wrinkles believed to have formed at the location of an invisible crack in the oxide layer. (d) Weave pattern. All scale bars 250 μm.

Another liquid, pyridine, results in the formation of "weave"-like wrinkle structures (Fig. 7d), which exist commingled amid regions of herringbone ordering. The process by which these weave patterns form is unknown, but is likely a result of rapid swelling kinetics. The observation of this rich spectrum of non-equilibrium patterns is highly encouraging, and inspires a wealth of new questions into the formation processes behind these "trapped" morphologies.

Conclusion

In this paper, we have presented experimental observations of wrinkles throughout a range of applied overstresses, enforced through control of the vapor pressure of a swelling agent for the wrinkling film. The applied overstress was quantified through beam bending experiments, which also served as confirmation that it is the swelling of the oxide film which drives wrinkle formation in UVO-treated PDMS. At low values of equibiaxial overstress, an array of dimples forms with clear hexagonal packing, instead of the checkerboard packing predicted by theory. As the overstress increases, the morphology transits to ridge-based patterns, both herringbone and labyrinth. Uniaxial ridge patterns form when the stress is non-equibiaxial due to a prestress applied before swelling. These findings highlight the importance of stress conditions on the formation of wrinkle patterns, a key consideration for applications hoping to take advantage of the spontaneous pattern generation enabled by surface wrinkling.

Experimental

General details

Crosslinked poly(dimethylsiloxane) (PDMS) was prepared from a commercial kit (Dow Sylgard 184) using a 10 : 1 prepolymer–crosslinker ratio and cured for a minimum of 2 hours at 70 °C. Samples for wrinkling were prepared with a minimum thickness of 3 mm. The prepared PDMS samples were exposed to UV–ozone oxidation (Jelight 342) for 10–60 minutes to form a stiff oxide on the surface.

Solvent vapor swelling

Oxidized PDMS samples were placed inside a sealed glass chamber along with a small volume (2–3 mL) of ethanol or ethanol–glycerol mixture. The amount of ethanol vapor in the atmosphere was estimated using ethanol–glycerol liquid–vapor data from the literature.[32] Optical microscopy (Zeiss Axiovert 300 m, 2.5–10× magnification) was used to characterize the wrinkled surfaces inside the chamber.

Clamped experiments

PDMS samples measuring 25 mm × 5 mm × 3 mm were fabricated and one end was placed into a mechanical clamp, decreasing the sample width locally. The clamped samples were treated with UVO, and then the clamp was removed. Upon removal, a differential stress developed between the oxidized film and the unmodified PDMS and varied spatially as a function of distance from the clamp. The stress distribution was confirmed by finite element models. These prestressed samples were then exposed to solvent vapor according to the process reported above.

Strain measurements

The applied strain due to differential swelling was measured by fabricating PDMS beams measuring 15 mm × 3 mm and ranging from 165–535 μm in thickness. The films were UVO-treated in the same manner as the wrinkling samples. After treatment, one end of each film was clamped between glass slides, with 12 mm extending beyond the clamp. The beams were then suspended vertically in sealed vapor chambers containing ethanol or ethanol–glycerol reservoirs. Due to volume loss during the UVO treatment, a slight curvature exists prior to swelling. Using a digital camera, the change in curvature was recorded and quantified as a function of time until no further change was recorded for a static ethanol–vapor concentration. The total time elapsed for these measurements was typically 20 minutes.

Acknowledgements

The authors wish to thank Prof. John Hutchinson, Prof. Zhigang Suo, and Shengqiang Cai for their fruitful discussions and helpful suggestions. The authors gratefully acknowledge the financial support of the National Science Foundation Materials Research Science and Engineering Center (MRSEC) on Polymers at the University of Massachusetts Amherst (NSF-DMR-0820506).

References

1 J. Genzer and J. Groenewold, *Soft Matter*, 2006, **2**, 310–323.
2 L. Pocivavsek, R. Dellsy, A. Kern, S. Johnson, B. Lin, K. Y. C. Lee and E. Cerda, *Science*, 2008, **320**, 912.
3 V. Trujillo, J. Kim and R. C. Hayward, *Soft Matter*, 2008, **4**, 564.
4 H. Mei, J. Y. Chung, C. M. Stafford, H.-H. Yu and R. Huang, *Appl. Phys. Lett.*, 2007, **90**, 151902.
5 L. Ponson, K. Diest, H. A. Atwater, G. Ravichandran and K. Bhattacharya, *J. Appl. Phys.*, 2009, **105**, 073514.
6 N. Bowden, S. Brittain, A. G. Evans, J. W. Hutchinson and G. M. Whitesides, *Nature*, 1998, **393**, 146.
7 A. Schweikart, A. Fortini, A. Wittemann, M. Schmidt and A. Fery, *Soft Matter*, 2010, **6**, 5860–5863.
8 M. Pretzl, A. Schweikart, C. Hanske, A. Chiche, U. Zettl, A. Horn, A. Böker and A. Fery, *Langmuir*, 2008, **24**, 12748.
9 T. Ohzono and H. Monobe, *Langmuir*, 2010, **26**, 6127.
10 M. Guvendiren and J. A. Burdick, *Biomaterials*, 2010, **31**, 6511.
11 E. P. Chan, E. J. Smith, R. C. Hayward and A. J. Crosby, *Adv. Mater.*, 2008, **20**, 711.
12 S. Kundu, C. S. Davis, T. Long, R. Sharma and A. J. Crosby, *J. Polym. Sci., Part B: Polym. Phys.*, 2011, **49**, 179.
13 E. P. Chan and A. J. Crosby, *Adv. Mater.*, 2006, **18**, 3238.
14 D. Chandra, P. Lin and S. Yang, *Appl. Phys. Lett.*, 2007, **91**, 251912.
15 M. Kücken and A. C. Newell, *J. Theor. Biol.*, 2005, **235**, 71.
16 L. Pocivavsek, B. Leahy, N. Holten-Andersen, B. Lin, K. Y. C. Lee and E. Cerda, *Soft Matter*, 2009, **5**, 1963.
17 E. Sharon, B. Roman, M. Marder, G.-S. Shin and H. L. Swinney, *Nature*, 2002, **419**, 579.
18 H. Liang and L. Mahadevan, *Proc. Natl. Acad. Sci. U. S. A.*, 2009, **106**, 22049.
19 J. Yin, Z. Cao, C. Li, I. Sheinman and X. Chen, *Proc. Natl. Acad. Sci. U. S. A.*, 2008, **105**, 19132.
20 H. G. Allen, *Analysis and Design of Structural Sandwich Panels*, Pergamon, New York, 1969.
21 P.-C. Lin and S. Yang, *Appl. Phys. Lett.*, 2007, **90**, 241903.
22 L. Mahadevan and S. Rica, *Science*, 2005, **307**(5716), 1740.
23 X. Chen and J. W. Hutchinson, *J. Appl. Mech.*, 2004, **71**(5), 597.
24 S. Cai, et al., Periodic patterns and energy states of buckled films on compliant substrates, *J. Mech. Phys. Solids*, 2011, DOI: 10.1016/j.jmps.2011.02.001.
25 B. Audoly and A. Boudaoud, *J. Mech. Phys. Solids*, 2008, **56**, 2444.
26 J. Song, H. Jiang, W. M. Choi, D. Y. Khang, Y. Huang and J. A. Rogers, *J. Appl. Phys.*, 2008, **103**, 014303.
27 Z. Huang, W. Hong and Z. Suo, *Phys. Rev. E: Stat., Nonlinear, Soft Matter Phys.*, 2004, **70**, 030601.
28 B. Audoly and A. Boudaoud, *J. Mech. Phys. Solids*, 2008, **56**, 2401.
29 D. Breid and A. J. Crosby, *Soft Matter*, 2009, **5**, 425.
30 M. Guvendiren, S. Yang and J. A. Burdick, *Adv. Funct. Mater.*, 2009, **19**, 3038.
31 J. Y. Chung, A. Nolte and C. Stafford, *Adv. Mater.*, 2009, **21**, 1.
32 W. Bachmann, *Z. Anorg. Allg. Chem.*, 1917, **100**, 1.
33 R. Huang and S. H. Im, *Phys. Rev. E: Stat., Nonlinear, Soft Matter Phys.*, 2006, **74**, 026214.
34 P. J. Yoo, K. Y. Suh, S. Y. Park and H. H. Lee, *Adv. Mater.*, 2002, **14**, 1383.
35 K. Efimenko, W. E. Wallace and J. Genzer, *J. Colloid Interface Sci.*, 2002, **254**, 306.
36 S. Timoshenko, *J. Opt. Soc. Am.*, 1925, **11**, 233.
37 F. Yang and J. C. M. Li, *J. Appl. Phys.*, 2003, **93**, 9304.
38 H. Vanderparre and P. Damman, *Phys. Rev. Lett.*, 2008, **101**, 124301.
39 J. Y. Cheng, C. A. Ross, H. I. Smith and E. L. Thomas, *Adv. Mater.*, 2006, **18**, 2505.
40 C. Li, A. Ji and Z. Cao, *Appl. Phys. Lett.*, 2007, **90**, 164102.
41 G. Cao, C. Li, A. Ji, Z. Cao and X. Chen, *Phys. Rev. Lett.*, 2008, **100**, 036102.
42 E. P. Chan and A. J. Crosby, *Soft Matter*, 2006, **2**, 324.
43 T. Ohzono and M. Shimomura, *Langmuir*, 2005, **21**, 7230.

